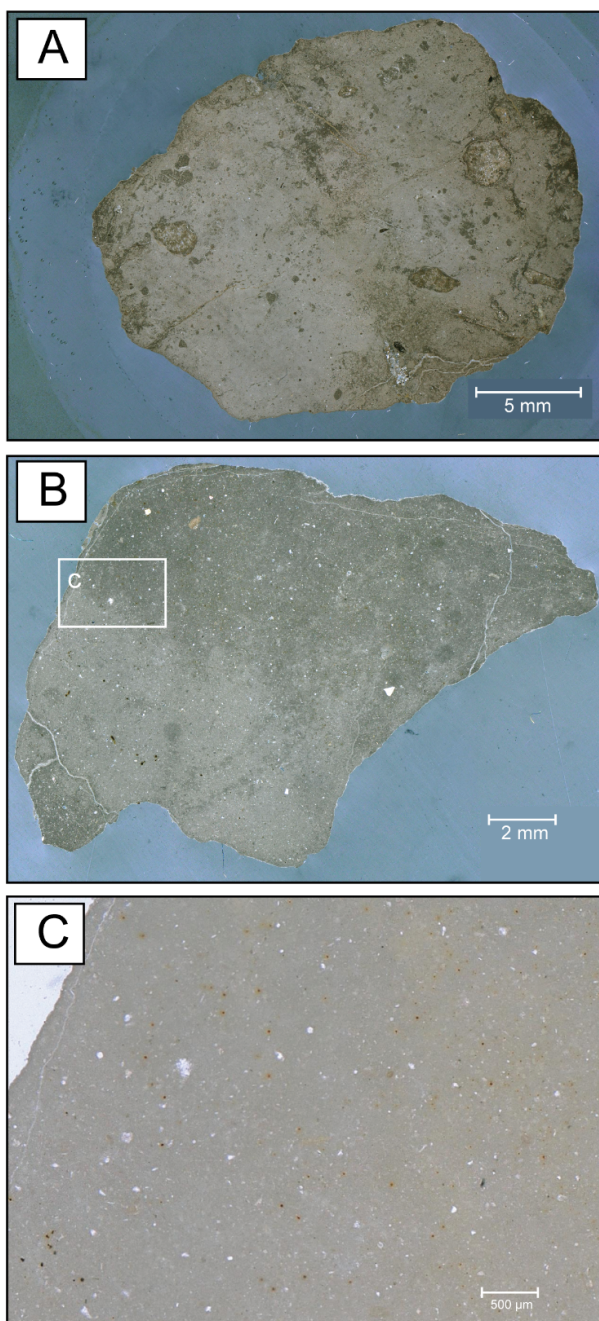


Supplementary Material

S1. Paleosols and pedogenic carbonate nodules in the Digne-Valensole basin

Calcite pedogenic carbonates nodules form commonly in soils of subhumid to semi-arid regions with well-defined wet-dry cycles over the year (Breecker et al., 2009). The formation process of pedogenic carbonates results from the dissolution of Ca-bearing minerals or eolian input. The latter release Ca^{2+} ions, which are subsequently transported downward and re-precipitate in various phases (Breecker et al., 2009; Quade et al., 2007; Zamanian et al., 2016). Carbonate precipitation and dissolution in soils are highly influenced by changes in soil temperature, moisture, and CO_2 that may vary daily or seasonally (Peters et al., 2013). While pedogenic carbonates tend to form during warm and dry seasons, it has been highlighted that carbonate formation can occur in different climates whenever the soil reaches supersaturation at different times of the year (Breecker et al., 2009; Gallagher et al., 2019). The use of pedogenic carbonate as a proxy in paleoclimate environment studies involves therefore considering implications of seasonal bias and comparing results with available analogous records (atmospheric CO_2 , $\delta^{18}\text{O}$ and $\delta^{13}\text{C}$ values).

The paleosols in the DVB developed in continental and coastal domains, the associated carbonate nodules formed therefore in floodplain and marshland deposits (Bialkowski, 2002). The carbonate content of the paleosols at the Châteauredon section is about 50% and can reach 90% in Bk horizons (Cojan et al., 2013). Carbonate nodules are abundant in the pedogenic horizon Bk as a result of downward migration from the above leaching horizon. The Châteauredon carbonate-bearing units, which developed on floodplain alluviums of the Digne-Valensole basin have a thickness ranging from a few meters to tens of meters (Fig. S3).



20

Figure S1: Typical examples of thin sections of pedogenic carbonate nodules with dominant micritic texture. (A) Sample 99CH14. (B) and (C) Sample 98GR29.

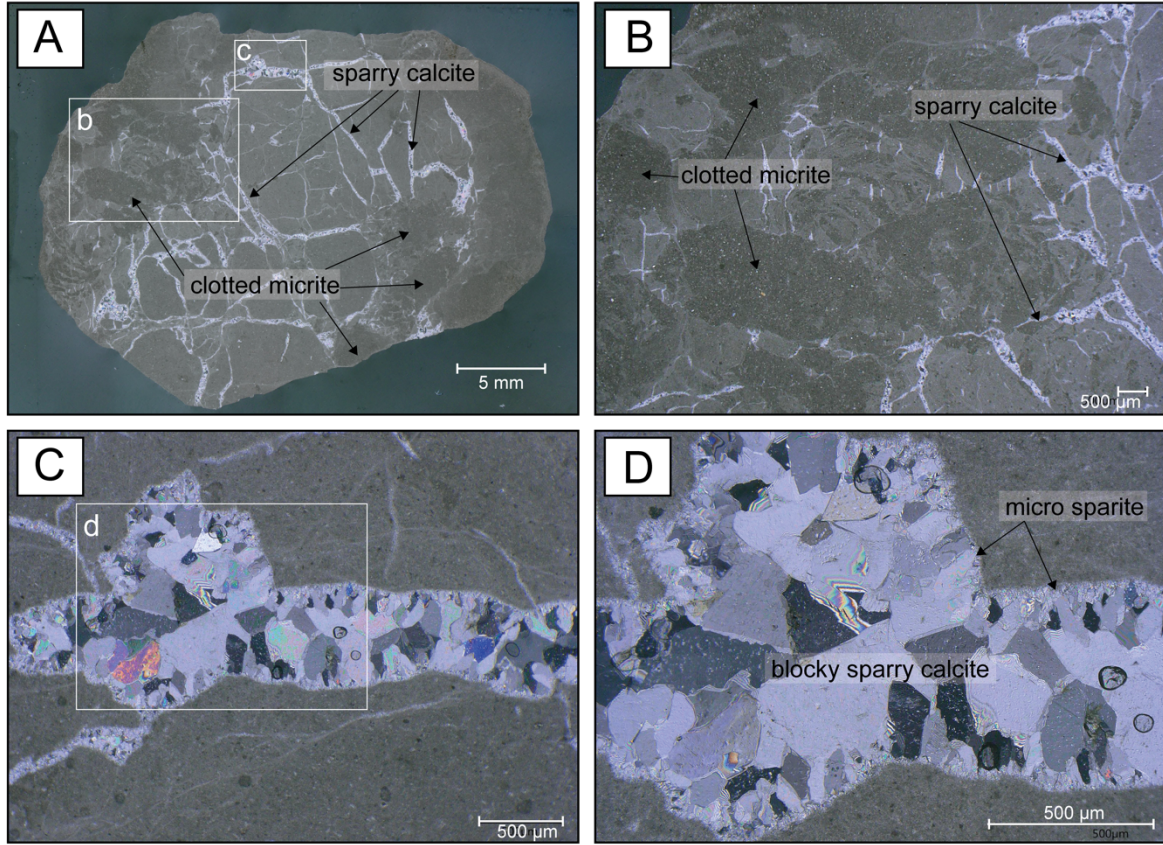


Figure S2: Microscopic images of a thin section from sample 98GR22. (A) and (B) depict a clotted micritic texture crosscut by sparry calcite veins, which might result from diagenetic alteration. (C) and (D) show a close-up of a sparry calcite vein. The sample is not considered in the discussion of our results because the Δ_{47} results likely represent a mixture of temperatures that reflect carbonate formation temperatures during soil formation (micritic calcite) and diagenesis (sparry calcite).

S2. Carbonate clumped isotope (Δ_{47}) measurements

Carbonate clumped isotope thermometry allows to determine the growth temperature of carbonate minerals (Ghosh et al., 2006; Eiler, 2011). The method relies on the determination of the temperature-dependent excess abundance of bonds between rare carbon and oxygen isotopes (^{13}C - ^{18}O) in the carbonate (Eiler, 2011). The clumped isotope value measures the excess of mass 47 isotopologues relative to a stochastic distribution in the CO_2 evolved from phosphoric acid digestion of carbonate, is reported as ' Δ_{47} '.

The Δ_{47} value can be expressed as:

$$\Delta_{47}(\text{‰}) = \left[\left(\frac{R^{47}}{R^{47*}} - 1 \right) \right] \times 1000$$

where R^i corresponds to the abundance ratio of masses 47 isotopologues relative to the abundance of mass 44 isotopologue, and R^{i*} is the expected stochastic ratio, predicted by the measured abundances of oxygen and carbon isotopes in the sample (Eiler and Schauble, 2004).

Geochemical data were acquired at the Joint Goethe University-Senckenberg BiK-F Stable Isotope Facility (Frankfurt, Germany). Measurements were made on a Kiel IV Carbonate Device paired to a MAT 253plus IRMS. Our analytical methods generally follow methodologies reported in previous work (Bernasconi et al., 2018; Müller et al., 2017; Tagliavento et al., 2023). The Kiel IV device was modified from its original configuration by adding two water sinks and a different heating-cooling system on the purification trap (see Tagliavento et al., 2023). After cutting and drilling each sample at low speed, for each replicate and depending on the carbonate content, 90 to 190 µg of powdered sample was reacted with 105% orthophosphoric acid at 70°C for 5 minutes starting from the last acid drop. In each sequence, ETH carbonate standards (Bernasconi et al., 2021) were measured for half of the analyses, with ETH 1, 2 and 3 run in a relative distribution of 1:1:2, and ETH4 analyzed less frequently and treated as an unknown sample. Raw intensity data was corrected for the negative pressure baseline using the $m/z_{47.5}$ signal and scaling factor method (Bernecker et al., 2023; Fiebig et al., 2021) applied on ETH-1 and ETH-2. Standardization was carried out by utilizing D47crunch (Daëron, 2021) in pooled sessions mode with ETH standards as carbonate anchors (Δ_{47}^{I-CDES} , Bernasconi et al., 2021). The resulting Δ_{47} values were converted into temperature using the calibration from Anderson et al. (2021):

$$\Delta_{47(I-CDES90^{\circ}C)} = 0.0391 \pm 0.0004 \times \frac{10^6}{T^2} + 0.154 \pm 0.0004$$

Each sample was measured in 8 to 18 replicates and the errors are reported as both fully propagated 68% (1SE) and 95% (2SE) confidence intervals.

Raw carbonate stable and clumped isotope data can be downloaded as supplementary Tables.

S3. Carbon and oxygen isotopic values

Carbon and oxygen isotopic values ($\delta^{13}C$ and $\delta^{18}O$) of the carbonate nodules were measured on the Kiel IV Carbonate Device. Raw data was anchored relative to nominal $\delta^{13}C$ and $\delta^{18}O$ reported for ETH1, ETH2 and ETH3 (Bernasconi et al., 2018) and are reported relative to VPDB.

Conversion to the SMOW scale was calculated following the equation of Kim et al. (2015):

$$\delta^{18}O_{VSMOW} (\text{‰}) = 1.03091 \times \delta^{18}O_{VPDB} + 30.92$$

Our $\delta^{13}C$ and $\delta^{18}O$ pedogenic carbonate values are in agreement with those reported by Bialkowski (2002).

S4. Oxygen isotopic values of soil water

The oxygen isotopic composition of the soil water ($\delta^{18}O_w$) from which the pedogenic carbonate formed was calculated for each nodule of the Digne-Valensole basin listed in Table 2.

The $\delta^{18}O_w$ values were calculated from the oxygen isotope composition of the carbonate ($\delta^{18}O_{SMOW}$) considering Δ_{47} -derived carbonate formation temperatures and the calcite-water oxygen isotope fractionation-temperature relationship of (Kim and O'Neil, 1997):

$$1000 \times \ln \alpha_{\text{calcite-water}} = \left(\frac{18.03 \times 10^3}{T} \right) - 32.42 \quad (4)$$

where T corresponds to the Δ_{47} -based carbonate formation temperature (in Kelvin).

75 **Table S1.** Section of origin (Les Granges, GR; Les Ruines, RU; Beynes, BE), depth (m), age (Ma), carbon ($\delta^{13}\text{C}$, ‰, vPDB) and oxygen ($\delta^{18}\text{O}$, ‰, vSMOW) stable isotope values and clumped isotopes measurements of the pedogenic carbonate nodules.

*Sample withdrawn

Sample ID	Interval	Section	Depth (m)	Age (Ma)	Age err. (Ma)	n	Δ_{47} CDES (‰)	$\pm \sigma$ (‰)	$\pm 1 \text{ SE}$ (‰)	T(Δ_{47}) (°C)	-1 SE (°C)'	+1 SE (°C)'	-2 SE (°C)'	+2 SE (°C)'	$\delta^{13}\text{C}$ (‰, vPDB)	$\delta^{18}\text{O}$ (‰, vSMOW)	$\delta^{18}\text{O}$ (‰, vSMOW)
99CH03	IV	GR	516	13.178	+0.1, -0.5	16	0.619	0.038	0.012	16.76	3.47	3.74	6.94	7.48	-9.9	23.67	-6.10
99CH01	IV	GR	510	13.365	0.1	13	0.607	0.083	0.014	20.51	4.11	4.49	8.22	8.98	-8.66	24.10	-4.88
99CH16	IV	GR	497	13.771	0.1	14	0.568	0.034	0.012	34.28	4.31	4.70	8.62	9.41	-6.15	25.19	-1.03
99CH14	III	GR	494.5	13.871	0.1	11	0.571	0.055	0.014	33.24	4.835	5.35	9.67	10.69	-8.24	26.10	-0.33
98GR34	III	GR	485.5	14.232	0.1	17	0.567	0.044	0.011	34.69	3.895	4.22	7.79	8.43	-6.24	24.59	-1.56
99CH10	III	GR	474.5	14.614	0.1	17	0.589	0.023	0.011	26.83	3.675	3.97	7.35	7.93	-6.28	24.95	-2.73
98GR29	III	GR	464.5	14.948	+0.1, -0.5	17	0.607	0.042	0.011	20.61	3.47	3.74	6.94	7.47	-6.56	24.85	-4.11
98GR24	III	GR	445.5	15.582	0.1	11	0.588	0.042	0.014	26.87	4.57	5.02	9.14	10.04	-6.9	24.95	-2.73
98GR22*	III*	GR*	442.5*	15.621*	0.1*	17*	0.555*	0.042*	0.011*	39.23*	4.065*	4.41*	8.13*	8.81*	-7.59*	24.78*	-0.52*
98GR22v*	III*	GR*	442.5*	15.621*	0.1*	-	-	-	-	-	-	-	-	-	-7.42*	24.94*	-
98GR18	III	GR	413	16.007	0.1	18	0.591	0.047	0.011	25.83	3.495	3.76	6.99	7.52	-6.74	24.99	-2.90
98GR08	II	GR	362	16.674	0.15	18	0.565	0.019	0.011	35.21	3.81	4.11	7.62	8.23	-6.86	24.77	-1.28
98GR02	II	GR	323.6	17.286	0.15	15	0.577	0.052	0.012	30.77	4.05	4.41	8.1	8.81	-7.14	24.65	-2.24
98RU32	II	RU	264.5	18.318	1.0	14	0.568	0.042	0.013	34.35	4.345	4.75	8.69	9.5	-7.32	23.76	-2.45
98RU30	II	RU	246.5	18.632	1.0	10	0.587	0.028	0.015	27.49	4.77	5.27	9.54	10.54	-7.38	24.11	-3.44
98RE46	I	BE	103	21.138	0.15	8	0.583	0.034	0.016	28.78	5.335	5.97	10.67	11.94	-7.74	24.30	-3.00
98RE30	I	BE	42	22.337	0.15	10	0.590	0.039	0.015	26.49	4.755	5.25	9.51	10.5	-7.48	23.95	-3.80

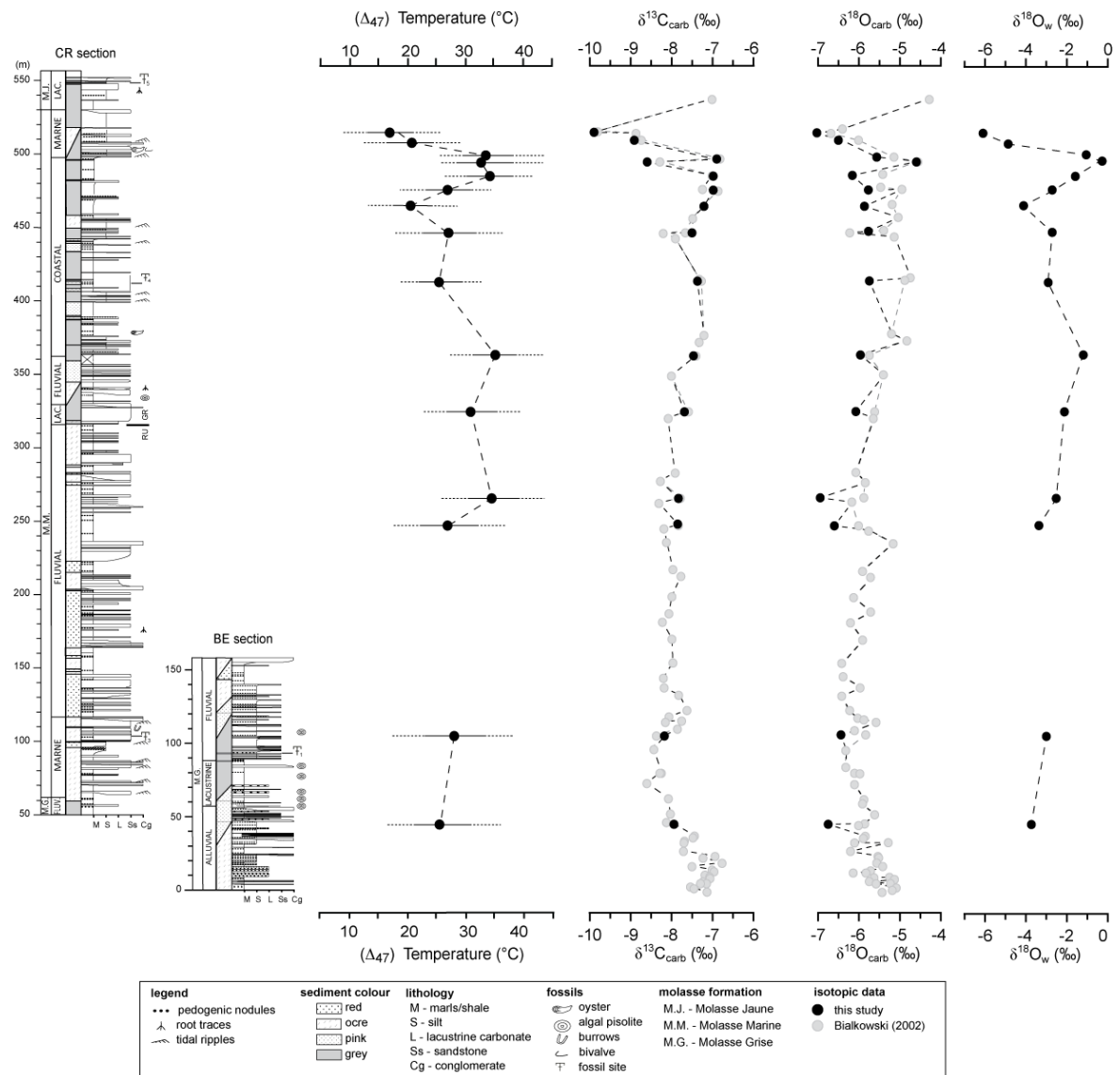


Figure S3: Pedogenic carbonate clumped isotope temperatures, oxygen and carbon stable isotopic values and calculated soil water $\delta^{18}\text{O}_w$ values. Lithostratigraphy of the Ruines-Grange (CR) and Beynes (BE) sections. Modified after Bauer (2006), Bialkowski (2002), and Cojan et al. (2013).

S5. Age Model

As described in the main text, we adopt and update the initial age model of Bialkowski et al. (2006) by tying the $\delta^{13}\text{C}$ curve of the BCR composite section to the LOESS smoothed benthic deep-sea foraminifera carbon isotope curve from Westerhold et al. (2020). Tuning of the curves was performed using the *QAnalySeries* software (Kotov and Paelike, 2018). Absolute ages for epochs and stages of Neogene follow the astronomically tuned time scale of Hilgen et al. (2012).

Table S2. Tie points age model GTS 2012

Tie point	Sample ID	GTS 1995 (Ma)	GTS 2012 (Ma)	Stratigraphic height (m)
12	98GR37	12.5	12.3	537.5
11	99CH03	13	13.1	516
10	99CH16	13.5	13.8	497
9	99CH14	14	13.9	494.5
8	98GR24	15.5	15.6	445.5
7	98GR05	16.9	16.8	348.5
6	98RU20	20.7	19.8	180.5
5	98RE45	21.8	21.3	93.8
4	98RE36	22.3	21.9	60
3	98RE31	22.8	22.3	43.5
2	98RE23	23	23	23.5
1	98RE05	23.3	23.3	-0.5

Table S3. Biostratigraphic, palynologic and dyncocyst-based constraints (from Bialkowski (2002) and Cojan et al. (2013) with stratigraphic height and age range.

Constraint	Stratigraphic height (m)	Age range (Ma)
Micromammal fossil F5	547	13.1–11.2
Pollen or dyncocyst (98GR38)	510	15.9–11.6
Pollen or dyncocyst (98GR34)	485.5	15.9–11.6
Pollen or dyncocyst (98GR27)	456.5	15.9–11.6
Pollen or dyncocyst (98GR25)	447	15.9–11.6
Pollen or dyncocyst (98GR24)	445.5	15.9–11.6
Micromammal fossil F4	407–417	17.1–16.7
Pollen or dyncocyst (98GR16)	375	17.5–15.1
Micromammal fossil F3	100–105	21.7–19.5
Micromammal fossil F1	95	21.7–19.5
Pollen or dyncocyst (RU3)	54.5	23.03–20.44

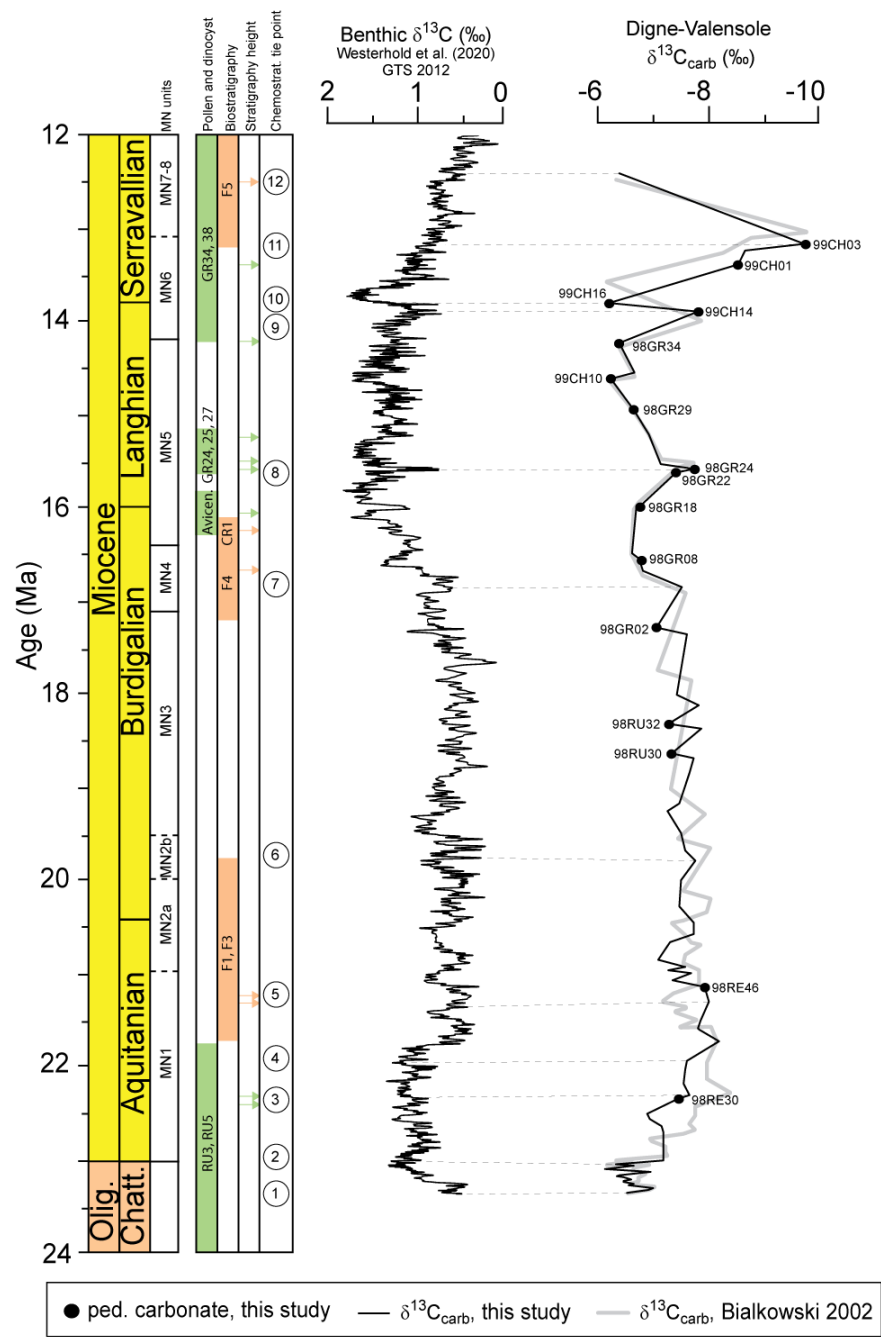


Figure S4: Correlation between the $\delta^{13}\text{C}$ curve of the BCR composite section (Bialkowski, 2002) and the reference marine data (Westerhold et al., 2020). Top left: European MN units with estimated ages (Hilgen et al., 2012): pollen and dinocyst records with estimated ages (Bialkowski et al., 2006); mammal biostratigraphy with estimated ages (Bialkowski et al., 2006;

Cojan et al., 2013); stratigraphic height at which the associated pollen/dinocyst or fossil was found in the section (orange and green arrows); tie point number (circled numbers; see Table S3).

110

References

- Anderson, N. T., Kelson, J. R., Kele, S., Daëron, M., Bonifacie, M., Horita, J., Mackey, T. J., John, C. M., Kluge, T., Petschnig, P., Jost, A. B., Huntington, K. W., Bernasconi, S. M., and Bergmann, K. D.: A Unified Clumped Isotope Thermometer Calibration (0.5–1,100°C) Using Carbonate-Based Standardization, *Geophys. Res. Lett.*, 48, 1–11, <https://doi.org/10.1029/2020GL092069>, 2021.
- Bauer, H.: Influence of climate , eustasy and tectonics in the architecture of continental deposits . a case study from the early and middle miocene of the digne-valensole foreland basin (se france), 2006.
- Bernasconi, S. M., Müller, I. A., Bergmann, K. D., Breitenbach, S. F. M., Fernandez, A., Hodell, D. A., Jaggi, M., Meckler, A. N., Millan, I., and Ziegler, M.: Reducing Uncertainties in Carbonate Clumped Isotope Analysis Through Consistent Carbonate-Based Standardization, *Geochemistry, Geophys. Geosystems*, 19, 2895–2914, <https://doi.org/10.1029/2017GC007385>, 2018.
- Bernasconi, S. M., Daëron, M., Bergmann, K. D., Bonifacie, M., Meckler, A. N., Affek, H. P., Anderson, N., Bajnai, D., Barkan, E., Beverly, E., Blamart, D., Burgener, L., Calmels, D., Chaduteau, C., Clog, M., Davidheiser-Kroll, B., Davies, A., Dux, F., Eiler, J., Elliott, B., Fetrow, A. C., Fiebig, J., Goldberg, S., Hermoso, M., Huntington, K. W., Hyland, E., Ingalls, M., Jaggi, M., John, C. M., Jost, A. B., Katz, S., Kelson, J., Kluge, T., Kocken, I. J., Laskar, A., Leutert, T. J., Liang, D., Lucarelli, J., Mackey, T. J., Manganot, X., Meinicke, N., Modestou, S. E., Müller, I. A., Murray, S., Neary, A., Packard, N., Passey, B. H., Pelletier, E., Petersen, S., Piasecki, A., Schauer, A., Snell, K. E., Swart, P. K., Tripathi, A., Upadhyay, D., Vennemann, T., Winkelstern, I., Yarian, D., Yoshida, N., Zhang, N., and Ziegler, M.: InterCarb: A Community Effort to Improve Interlaboratory Standardization of the Carbonate Clumped Isotope Thermometer Using Carbonate Standards, *Geochemistry, Geophys. Geosystems*, 22, 1–25, <https://doi.org/10.1029/2020GC009588>, 2021.
- Bernecker, M., Hofmann, S., Staudigel, P. T., Davies, A. J., Tagliavento, M., Meijer, N., Ballian, A., and Fiebig, J.: A robust methodology for triple ($\Delta 47$, $\Delta 48$, $\Delta 49$) clumped isotope analysis of carbonates, *Chem. Geol.*, 642, 121803, <https://doi.org/10.1016/j.chemgeo.2023.121803>, 2023.
- Bialkowski, A.: Stratigraphie isotopique (carbone et oxygène) des séries continentales d’un bassin d’avant-pays (Oligo-Miocène du bassin de Digne-Valensole): paléoenvironnements et séquences de dépôt, *École Nationale Supérieure des Mines de Paris*, 2002.
- Bialkowski, A., Châteauneuf, J. J., Cojan, I., and Bauer, H.: Integrated stratigraphy and paleoenvironmental reconstruction of the Miocene series of the Châteauredon Dome, S.E. France, *Eclogae Geol. Helv.*, 99, 1–15, <https://doi.org/10.1007/s00015-006-1176-y>, 2006.
- Breecker, D. O., Sharp, Z. D., and McFadden, L. D.: Seasonal bias in the formation and stable isotopic composition of pedogenic carbonate in modern soils from central New Mexico, USA, *Bull. Geol. Soc. Am.*, 121, 630–640, <https://doi.org/10.1130/B26413.1>, 2009.

- Cojan, I., Bialkowski, A., Gillot, T., and Renard, M.: Paleoenvironnement and paleoclimate reconstruction for the
145 early to middle Miocene from stable isotopes in pedogenic carbonates (Digne-Valensole basin, southeastern France), *Bull. la Soc. Geol. Fr.*, 184, 583–599, <https://doi.org/10.2113/gssgfbull.184.6.583>, 2013.
- Daëron, M.: Full Propagation of Analytical Uncertainties in $\Delta 47$ Measurements, *Geochemistry, Geophys. Geosystems*, 22, 1–19, <https://doi.org/10.1029/2020GC009592>, 2021.
- Eiler, J. M.: Paleoclimate reconstruction using carbonate clumped isotope thermometry, *Quat. Sci. Rev.*, 30, 3575–
150 3588, <https://doi.org/10.1016/j.quascirev.2011.09.001>, 2011.
- Fiebig, J., Daëron, M., Bernecker, M., Guo, W., Schneider, G., Boch, R., Bernasconi, S. M., Jautzy, J., and Dietzel, M.: Calibration of the dual clumped isotope thermometer for carbonates, *Geochim. Cosmochim. Acta*, 312, 235–256, <https://doi.org/10.1016/j.gca.2021.07.012>, 2021.
- Gallagher, T. M., Hren, M., and Sheldon, N. D.: The effect of soil temperature seasonality on climate
155 reconstructions from paleosols, *Am. J. Sci.*, 319, 549–581, <https://doi.org/10.2475/07.2019.02>, 2019.
- Hilgen, F. J., Lourens, L. J., Van Dam, J. A., Beu, A. G., Boyes, A. F., Cooper, R. A., Krijgsman, W., Ogg, J. G., Piller, W. E., and Wilson, D. S.: The neogene period, 923–978 pp., <https://doi.org/10.1016/B978-0-444-59425-9.00029-9>, 2012.
- Kim, S. T. and O’Neil, J. R.: Equilibrium and nonequilibrium oxygen isotope effects in synthetic carbonates,
160 *Geochim. Cosmochim. Acta*, 61, 3461–3475, [https://doi.org/10.1016/S0016-7037\(97\)00169-5](https://doi.org/10.1016/S0016-7037(97)00169-5), 1997.
- Kim, S. T., Coplen, T. B., and Horita, J.: Normalization of stable isotope data for carbonate minerals: Implementation of IUPAC guidelines, *Geochim. Cosmochim. Acta*, 158, 276–289, <https://doi.org/10.1016/j.gca.2015.02.011>, 2015.
- Kotov, S. and Paelike, H.: QAnalySeries - a cross-platform time series tuning and analysis tool, in: AGU Fall
165 Meeting Abstracts, PP53D-1230, 2018.
- Müller, I. A., Fernandez, A., Radke, J., van Dijk, J., Bowen, D., Schwieters, J., and Bernasconi, S. M.: Carbonate clumped isotope analyses with the long-integration dual-inlet (LIDI) workflow: scratching at the lower sample weight boundaries, *Rapid Commun. Mass Spectrom.*, 31, 1057–1066, <https://doi.org/10.1002/rcm.7878>, 2017.
- Peters, N. A., Huntington, K. W., and Hoke, G. D.: Hot or not? Impact of seasonally variable soil carbonate
170 formation on paleotemperature and O-isotope records from clumped isotope thermometry, *Earth Planet. Sci. Lett.*, 361, 208–218, <https://doi.org/10.1016/j.epsl.2012.10.024>, 2013.
- Quade, J., Garzzone, C., and Eiler, J.: Paleoelevation reconstruction using pedogenic carbonates, *Paleoaltimetry Geochemical Thermodyn. Approaches*, 66, 53–87, <https://doi.org/10.2138/rmg.2007.66.3>, 2007.
- Tagliavento, M., Hofmann, S., Böttcher, M. E., Peltz, M., and Fiebig, J.: Clumped isotope analysis of (bio)
175 apatite using a Kiel IV device in long-integration dual-inlet mode, *Rapid Commun Mass Spectrom.*, 37, 1–14, <https://doi.org/10.1002/rcm.9656>, 2023.
- Westerhold, T., Marwan, N., Drury, A. J., Liebrand, D., Agnini, C., Anagnostou, E., Barnet, J. S. K., Bohaty, S. M., De Vleeschouwer, D., Florindo, F., Frederichs, T., Hodell, D. A., Holbourn, A. E., Kroon, D., Lauretano, V., Littler, K., Lourens, L. J., Lyle, M., Pälike, H., Röhl, U., Tian, J., Wilkens, R. H., Wilson, P. A., and Zachos, J.

180 C.: An astronomically dated record of Earth's climate and its predictability over the last 66 million years, *Science* (80-.), 369, 1383–1388, <https://doi.org/10.1126/SCIENCE.ABA6853>, 2020.

Zamanian, K., Pustovoytov, K., and Kuzyakov, Y.: Pedogenic carbonates: Forms and formation processes, *Earth-Science Rev.*, 157, 1–17, <https://doi.org/10.1016/j.earscirev.2016.03.003>, 2016.